RESEARCH/REVIEW ARTICLE

The impact of a thermodynamic sea-ice module in the COSMO numerical weather prediction model on simulations for the Laptev Sea, Siberian Arctic

David Schröder,[1,2] Günther Heinemann[1] & Sascha Willmes[1]

1 Department of Environmental Meteorology, University of Trier, Behringstr. 21, DE-54286 Trier, Germany
2 Centre for Polar Observation and Modelling, University College London, Gower Street, WC1E 6BT London, UK

Keywords
Laptev Sea; polynya; mesoscale modelling.

Correspondence
David Schröder, Department of Environmental Meteorology, University of Trier, Behringstr. 21, DE-54286 Trier, Germany.
E-mail: david.schroeder@uni-trier.de

Abstract

Previous versions of the Consortium for Small-scale Modelling (COSMO) numerical weather prediction model have used a constant sea-ice surface temperature, but observations show a high degree of variability on sub-daily timescales. To account for this, we have implemented a thermodynamic sea-ice module in COSMO and performed simulations at a resolution of 15 km and 5 km for the Laptev Sea area in April 2008. Temporal and spatial variability of surface and 2-m air temperature are verified by four automatic weather stations deployed along the edge of the western New Siberian polynya during the Transdrift XIII-2 expedition and by surface temperature charts derived from Moderate Resolution Imaging Spectroradiometer (MODIS) satellite data. A remarkable agreement between the new model results and these observations demonstrates that the implemented sea-ice module can be applied for short-range simulations. Prescribing the polynya areas daily, our COSMO simulations provide a high-resolution and high-quality atmospheric data set for the Laptev Sea for the period 14–30 April 2008. Based on this data set, we derive a mean total sea-ice production rate of 0.53 km^3/day for all Laptev Sea polynyas under the assumption that the polynyas are ice-free and a rate of 0.30 km^3/day if a 10-cm-thin ice layer is assumed. Our results indicate that ice production in Laptev Sea polynyas has been overestimated in previous studies.

The Laptev Sea (Fig. 1) is characterized by flaw polynyas that occur at the edge of the fast ice surrounding the coastal zones during wintertime (Zakharov 1996; Dethleff et al. 1998; Bareiss & Görgen 2005). Polynyas are large regions of open water or thin ice that reappear regularly at the same location (Barber & Massom 2007). There are five polynyas in the Laptev Sea: the eastern Severnaya Zemlya polynya, the north-eastern Taimyr polynya and the Taimyr polynya in the western part; the Anabar–Lena polynya in the southern part; and the western New Siberian polynya in the eastern part (Bareiss & Görgen 2005; see fig. 1 in Willmes et al. 2011 [this volume] for locations). Due to large turbulent atmospheric heat fluxes, polynyas are strong sea-ice producers (e.g., Barber & Massom 2007). Among the 61 recurring polynyas indentified by Barber & Massom (2007) in the Arctic, the Laptev Sea polynyas play a key role for the Arctic sea-ice budget due to the sizable ice export (annual area export between 250 000 and 750 000 km^2) from the Laptev Sea to the central Arctic (Rigor & Colony 1997; Dethleff et al. 1998; Alexandrov et al. 2000). However, estimates of sea-ice production in the Laptev Sea polynyas (Rigor & Colony 1997; Dethleff et al. 1998; Alexandrov et al. 2000) are arguably constrained due to a lack of high-resolution, high-quality atmospheric data.

In the current version of the Consortium for Small-scale Modelling (COSMO) numerical weather prediction (NWP) model (Steppeler et al. 2003; Schättler et al. 2008), sea-ice surface temperature is constant with time, but observations show a high degree of

Citation: *Polar Research* 2011, *30*, 6334, DOI: 10.3402/polar.v30i0.6334

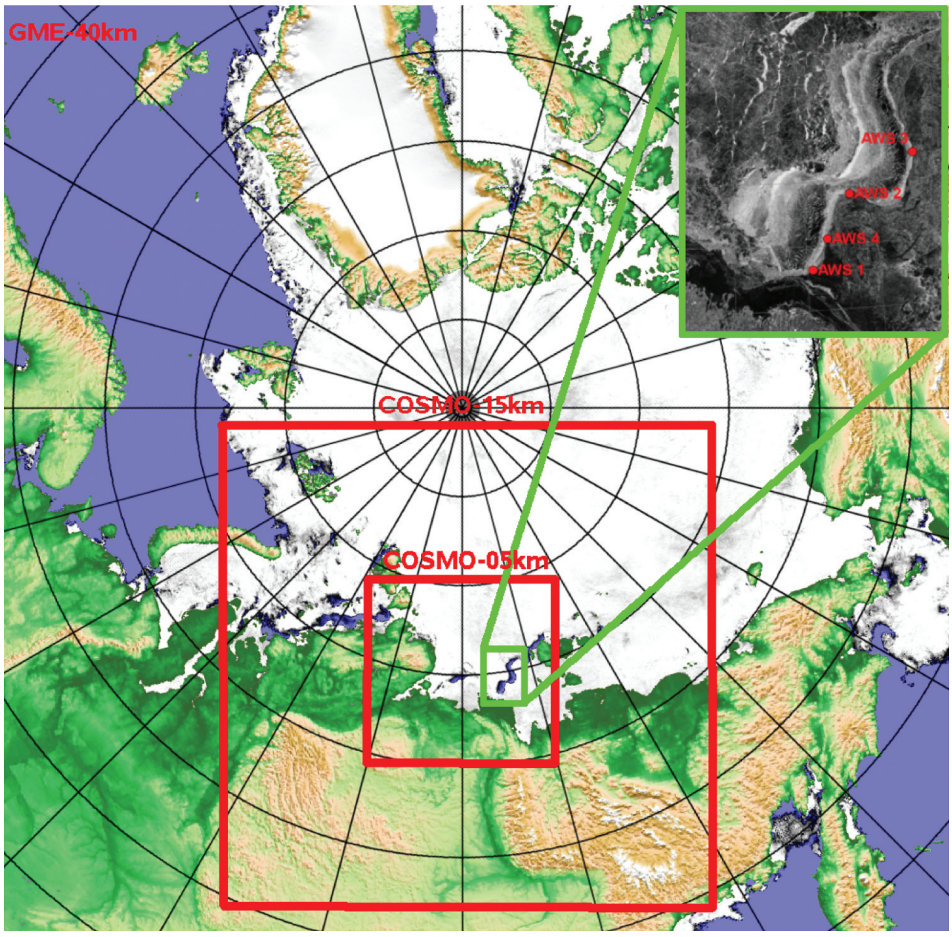

Fig. 1 Locations of the model domains COSMO-15km and COSMO-05km in the Laptev Sea. The underlying map (source: www.seaice.de) shows the sea-ice concentration (white for 100% ice and blue for open water; data from the Advanced Microwave Scanning Radiometer–Earth Observing System) on 29 April 2008. The position of the four automatic weather stations (AWS) are shown in the small map in the right top corner (Advanced Synthetic Aperture Radar image, 30 April 2008).

variability on sub-daily timescales. For example, changes of 20 K within 24 hours were measured over relatively thin ice (ca. 30 cm) in the Baltic Sea (Brümmer et al. 2002). We implement a thermodynamic sea-ice module in COSMO to extend the utility of the non-hydrostatic atmospheric model to process studies over sea-ice regions.

The following sections introduce the COSMO model, the implementation of the sea-ice module and the design of the simulations. To verify our simulations we apply in situ measurements and remote-sensing data for the Laptev Sea. We undertake a detailed verification of the temporal and spatial variability of sea-ice surface temperature. Finally, we apply COSMO—with the sea-ice module—to provide high-resolution atmospheric data for the Laptev Sea in April 2008 and to calculate the sea-ice production in the polynyas.

The NWP model COSMO

The COSMO model is a non-hydrostatic, limited-area atmospheric prediction model (Steppeler et al. 2003; Schättler et al. 2008). It has been the operational weather prediction model of the German Weather Service since 1999—in the earlier years under the name "Lokal-Modell" (LM). It has a horizontal resolution of 2.8 km for Germany and 7 km for Europe. The COSMO model is based on the primitive thermo-hydrodynamical equations that are solved on a staggered Arakawa C/Lorenz grid applied on a rotated spherical coordinate system. It is designed not only for NWP, but also for various scientific applications on the mesoscale, ranging from case studies over a few hours to climate simulations over decades. Users determine model domain and resolution and choose parameterization schemes according to their requirements (Schättler et al. 2008).

Citation: *Polar Research* 2011, *30*, 6334, DOI: 10.3402/polar.v30i0.6334

In our studies we have made the following selections. For time integrations we apply both a third-order Runge-Kutta scheme (Wicker & Skamarock 2002) and a three-time-level Leapfrog scheme, which is a variant of the Klemp & Wilhelmson (1978) scheme. Radiation processes are calculated hourly using the Ritter & Geleyn (1992) scheme. The Tiedtke (1989) scheme is used for moisture convection. The vertical diffusion is calculated by a level-2.5 closure scheme based on a prognostic equation for turbulent kinetic energy. For the parameterization of surface fluxes, we tested a bulk transfer scheme with stability and roughness dependence based on Louis (1979) and the recommended surface scheme based on the turbulent kinetic energy. Due to better results over sea ice, we apply the bulk scheme. Soil temperature and water content are calculated using the eight-layer soil model TERRA-ML (Heise et al. 2006).

Several European countries have participated in the development and improvement of the COSMO model. Since most applications have been made for Central Europe thus far (e.g., Elementi et al. 2005; Grützun et al. 2008; Muhlbauer & Lohmann 2008; Stephan et al. 2008), there is no sea-ice parameterization in the current version. In the simulations that were performed for polar regions (Klein et al. 2001; Wacker et al. 2005; Hebbinghaus & Heinemann 2006), a constant sea-ice surface temperature was assumed. COSMO has been operationally used since 2008 by the Russian Hydrometeorology Service for Russia including the adjacent Arctic seas, where sea ice plays an important role. In order to simulate the surface layer over sea ice more realistically, we implemented a simple and efficient thermodynamic sea-ice module.

Implementation of a sea-ice module

Option A: sea ice without snow cover

We essentially adopt the one-layer sea-ice module of the global NWP Global Model Extended system (GME) of the German Weather Service (Mironov & Ritter 2004). Changes of sea-ice surface temperature T_{sfc} are calculated on the basis of the energy budget of the ice layer:

$$\frac{\partial T_{sfc}}{\partial t} = \frac{1}{c_* \cdot h_i}\left[\frac{Q_A + Q_I}{\rho_i \cdot c_i}\right], \tag{1}$$

with

Q_A, the total atmospheric heat flux (sum of surface net radiation balance and turbulent surface fluxes of sensible and latent heat);

Q_I, the conductive heat flux at the bottom of the ice layer;

ρ_i, the density of sea ice ($\rho_i = 910$ kg m^3);

c_*, the empirical shape factor;

c_i, the heat capacity of sea ice ($c_i = 2100$ J kg^{-1} K^{-1}); and

h_i, the ice thickness.

All heat fluxes have a positive sign when directed to the respective surface. In order to account for the temperature profile, an empirical shape factor c_* is introduced. From an energetic point of view, the applied value of $c_* = 0.5$ (based on Mironov & Ritter 2004) means that T_{sfc} is valid for the upper half of the ice layer and T_{oi} for the lower half. Thus, T_{sfc} is not only the ice-surface temperature but also an ice-volume temperature.

The conductive heat flux at the bottom of the ice layer Q_I is approximated using a linear approach:

$$Q_I = \frac{\lambda_i (T_{afc} - T_{oi})}{h_i}, \tag{2}$$

with

T_{oi}, the temperature at the bottom of the sea-ice layer ($T_{oi} = -1.8^\circ$C);

T_{sfc}, the temperature at the top of the sea-ice layer; and

λ_i, the heat conductivity of sea ice ($\lambda_i = 2.3$ W m^{-1} K^{-1}).

The conductive heat flux is not vertically constant due to the heat capacity of sea ice that is accounted for.

Equation 1 is only valid for ice temperatures $T_{sfc} \leq 0^\circ$C. For this temperature range, the growth rate is calculated on the basis of the energy balance at the sea-ice–ocean interface:

$$\frac{\partial h_i}{\partial t} = \frac{Q_I + Q_W}{\rho_i \cdot L_f}, \tag{3a}$$

with

Q_W, the turbulent ocean heat flux; and

L_f, the latent heat of freezing ($L_f = 0.334\ 10^6$ J kg^{-1}).

If the ice surface temperature reaches 0°C and the total atmospheric heat flux is positive, additional melting takes place:

$$\frac{\partial h_i}{\partial t} = \frac{Q_I + Q_W}{\rho_i \cdot L_f} - \frac{Q_A}{\rho_i \cdot L_f}. \tag{3b}$$

The turbulent fluxes of sensible and latent heat are calculated by COSMO's surface layer transfer scheme. A roughness length for sea ice of $z_{0\_i} = 5$ mm is applied. For the shortwave radiation fluxes an albedo of $alb_i = 0.7$ is assumed. If the sea ice melts to a height of less than 5 cm, open-water settings are applied with an albedo of 0.07 and a roughness length calculated by a modified Charnock formula (Charnock 1955).

Option B: sea ice with snow cover

This module accounts for the different thermal characteristics of snow. It is a simple approach to simulate a realistic surface temperature over sea ice that is covered by snow on short-range forecasts up to several days. This approach is not appropriate for climate simulations. If snow is present (minimum height of 5 cm), we assume the temperature between the snow and ice layer to be constant with time. The GME surface temperature or external data can be applied. We can calculate the conductive heat flux and the change of surface temperature with the same equations as above but using the thermal characteristics of snow:

$$Q_S = \frac{\lambda_s (T_{sfc} - T_{si})}{h_s}, \quad (4)$$

with

λ_s, the heat conductivity of snow ($\lambda_s = 0.7$ W m^{-1} K^{-1}); and

h_s, the snow height,

and

$$\frac{\partial T_{sfc}}{\partial t} = \frac{1}{c_* \cdot h_s} \left[\frac{Q_A + Q_S}{\rho_s \cdot c_s} \right], \quad (5)$$

with

T_{si}, the temperature at the interface between snow and ice;

ρ_s, the density of snow ($\rho_s = 300$ kg m^3);

c_s, the heat capacity of snow ($c_s = c_i = 2100$ J kg^{-1} K^{-1}); and

c_*, the shape factor.

To optimize the response time of ice surface temperature to the atmospheric heat flux, we apply a value for the heat conductivity of snow of $\lambda_s = 0.7$ W m^{-1} K^{-1}, which is larger than the standard value of 0.3 W m^{-1} K^{-1} (e.g., Timmermann et al. 2002) and theoretically corresponds to a density of snow of $c_s = 520$ kg m^3 (Male 1980).

Design of the simulations

The model simulations are performed by means of a model chain consisting of the six-hourly global GME analyses of the German Weather Service with a mesh size of 40 km (Majewski et al. 2002), COSMO runs with a mesh size of 15 km for a 3000 km × 3000 km area surrounding the Laptev Sea (COSMO-15 km) and COSMO runs with a mesh size of 5 km for a 1000 km × 1000 km area covering only the Laptev Sea (COSMO-05 km). The locations of the model domains are shown in Fig. 1. The initial sea-ice conditions are derived from sea-ice concentrations, based on microwave brightness temperature of the Advanced Microwave Scanning Radiometer–Earth Observing System (AMSR-E; Spreen et al. 2008). Grid cells with a sea-ice concentration of more than 70% are treated as sea-ice grid points and grid cells with a sea-ice concentration of less than 70% are treated as open-water grid cells. This is a common threshold for polynya classification (Massom et al. 1998; Parmiggiani 2006). A homogeneous initial sea-ice thickness of 1 m is assumed. The elevation of the land surface is taken from the Global Land One-kilometer Base Elevation digital elevation model and soil type from the Food and Agriculture Organization data set provided by the US National Aeronautics and Space Administration (NASA). The COSMO-15 km runs are started with GME analyses as atmospheric initial data and are nested into the GME analyses every six hours. The COSMO-05 km runs are started with the COSMO-15 km data and nested into the COSMO-15 km data every hour. In both cases, two nesting grid cells are applied.

COSMO-ice

Applying the sea-ice module Option A, we obtain 17 COSMO-15 km and COSMO-05 km simulations that cover the period from 13 April until 29 April 2008, starting at 00 UTC daily and each lasting 30 hours. For each run, a new initial sea-ice distribution is applied. Omitting the first six hours of each run for spin-up reasons and merging all runs together, we obtain a three-dimensional data set for the period 14 April 00 UTC until 30 April 00 UTC.

COSMO-ice-5 days

Applying the sea-ice module Option A, we obtain a five-day run starting on 14 April 2008 with a mesh size of 15 km.

COSMO-snow

We use the same procedure as for COSMO-ice, but apply the sea-ice module Option B including snow treatment. A snow height of 10 cm is applied uniformly based on measurements along the western New Siberian polynya (see below).

COSMO-snow-5 days

Applying the sea-ice module Option B, we obtain a five-day run starting on 14 April 2008 with a mesh size of 15 km.

Citation: *Polar Research* 2011, *30*, 6334, DOI: 10.3402/polar.v30i0.6334

Table 1 Comparison between observed (automatic weather stations [AWS]) and analysed (Global Model Extended system [GME]) wind speed at 10 m: mean values, bias, root mean square error (RMSE) and correlation coefficient (*r*). Statistics are calculated from six-hourly data from 12 to 30 April 2008. The wind speed was measured at a height of 3 m, but was transformed to a height of 10 m assuming neutral stratification.

Wind speed in m s^{-1}	Mean (AWS)	Mean (GME)	Bias	RMSE	*r*
AWS 1	4.3	4.2	+0.1	1.3	0.73
AWS 2	4.1	4.5	+0.4	1.4	0.86
AWS 3	4.0	4.3	+0.3	1.4	0.85
AWS 4	5.2	5.5	+0.3	0.8	0.80

COSMO-snow-pol10

We used the same procedure as for COSMO-snow, but with the assumption that polynyas are covered by a snow-free layer of ice that is 10-cm thick. Thus, Option A is applied over the polynyas and Option B over the thicker sea ice.

In situ and satellite data

During the Transdrift XIII-2 expedition from 11 April to 29 April 2008 four automatic weather stations (AWS) were deployed along the edge of the western New Siberian Polynya (Fig. 1; Heinemann et al. 2009). Wind speed and direction were observed at a height of 3 m with an accuracy of 2% in speed and 3° in direction. Air temperature and relative humidity were measured at a height of 2 m with an accuracy of 0.5 K and 4%, respectively. The measured barometric pressure has an accuracy of 1 hPa. In addition, net radiation was measured by a net radiometer with an accuracy of 5 Wm^{-2}. All data have been calibrated and validated during post-processing (Heinemann et al. 2009). Here, we apply hourly data.

Daily sea-ice concentration data were obtained from the University of Hamburg (Spreen et al. 2008). Surface temperatures were derived from the Moderate Resolution Imaging Spectroradiometer (MODIS) Level 1B calibrated radiances, provided by the NASA Level 1 and Atmosphere Archive and Distribution System (LAADS). Based on MODIS thermal infrared data, surface temperatures were calculated following the split-window method of Key et al. (1997).

Verification: results for the Laptev Sea

Quality of the GME analyses

Results of limited area model studies depend strongly on the accuracy of initial and boundary data (e.g., Rinke & Dethloff 2001). The applied GME analyses are known to be accurate for Europe, but the Laptev Sea is an area with sparse observations. The four AWS deployed during Transdrift XIII-2 enable us to verify sea-level pressure, near-surface air temperature, humidity and wind speed. Our observations did not enter into the GME analyses scheme and they therefore compose an independent data set. Example time series of 10-m wind speed and 2-m air temperature are shown in Fig. 2 for AWS 2. To take into account that a point measurement does not generally represent a grid cell mean, the values for the eight surrounding grid cells are shown in addition to the nearest grid cell. The differences between observed and GME wind speed are mainly below 1 ms^{-1} (Fig. 2a). The same is true for the other three AWS (not shown). The biases are below 0.4 ms^{-1} (Table 1) for all four AWS, the correlation coefficients range from 0.73 to 0.86, and the root mean square (RMS) errors from 0.8 ms^{-1} to 1.4 ms^{-1}. The RMS values for six-hourly GME data are remarkably low compared with general RMS errors for daily and monthly reanalysis products, which vary between 1 and 2 ms^{-1} (Bromwich & Wang 2005; Kolstad 2008; Bentamy et al. 2009). The comparison reveals that the synoptic weather situation is well captured by the GME analyses for the Laptev Sea during this period. This is confirmed by an agreement between observed and GME sea-surface pressure (not shown).

However, there are large discrepancies between observed and GME air temperatures (Fig. 2b). Though the whole-period means hardly differ, the sub-daily variations are underestimated by an order of magnitude. For AWS 2 the mean observed diurnal cycle amounts to 6.0 K (based on six-hourly data), whereas the mean diurnal cycle in the analyses only amounts to 0.7 K. This cannot be explained by local effects because the other AWS show a comparable diurnal cycle of 5.5 K, 6.6 K and 5.4 K and the surrounding GME grid points do not differ more than 0.5 K from the nearest grid point. The missing diurnal cycle of 2-m air temperature is likely to be caused by the sea-ice parameterization scheme in the GME.

Impact of sea-ice parameterization on temporal variability

For verification of the two different sea-ice parameterization schemes, we compare our model results (COSMO-

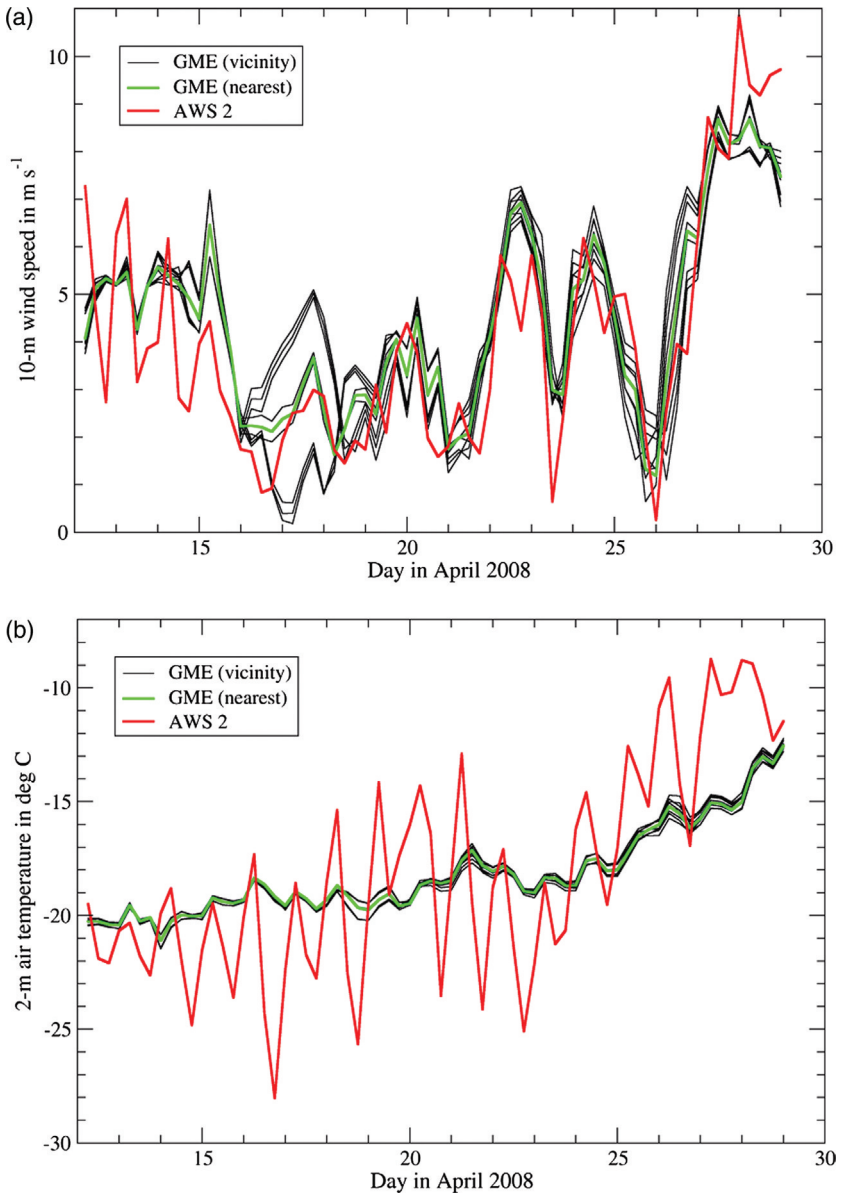

Fig. 2 Comparison of (a) 10-m wind speed and (b) 2-m air temperature between automatic weather station (AWS) 2 observations and the Global Model Extended system (GME) analyses for the period 12–30 April 2008. The green line represents the nearest grid point; black lines surround eight grid points. The wind speed was measured at a height of 3 m, but was transformed to a height of 10 m assuming neutral stratification.

05km runs) with the observed 2-m air temperature in the Laptev Sea. It cannot be assumed that the observations close to the polynya edge are representative for whole-model grid cells during the strong polynya event starting on 26 April 2008. Therefore, the verification time is restricted to the period 14–25 April 2008.

2-m air temperature. Temperature time series are shown for the location of AWS 2 in Fig. 3a. The observed variability of the 2-m temperature is not simulated by the COSMO-ice runs. Instead, the simulated air temperature closely follows the GME analyses because the same sea-ice parameterization scheme has been applied. A shift of about 2 K occurs, probably due to ice-thickness differences: in the GME analyses the sea-ice thickness amounts to approximately 2.5 m whereas in COSMO-ice a more realistic value of 1 m is applied.

A realistic simulation of the variability of 2-m air temperature can be achieved by taking into account a

Citation: *Polar Research* 2011, *30*, 6334, DOI: 10.3402/polar.v30i0.6334

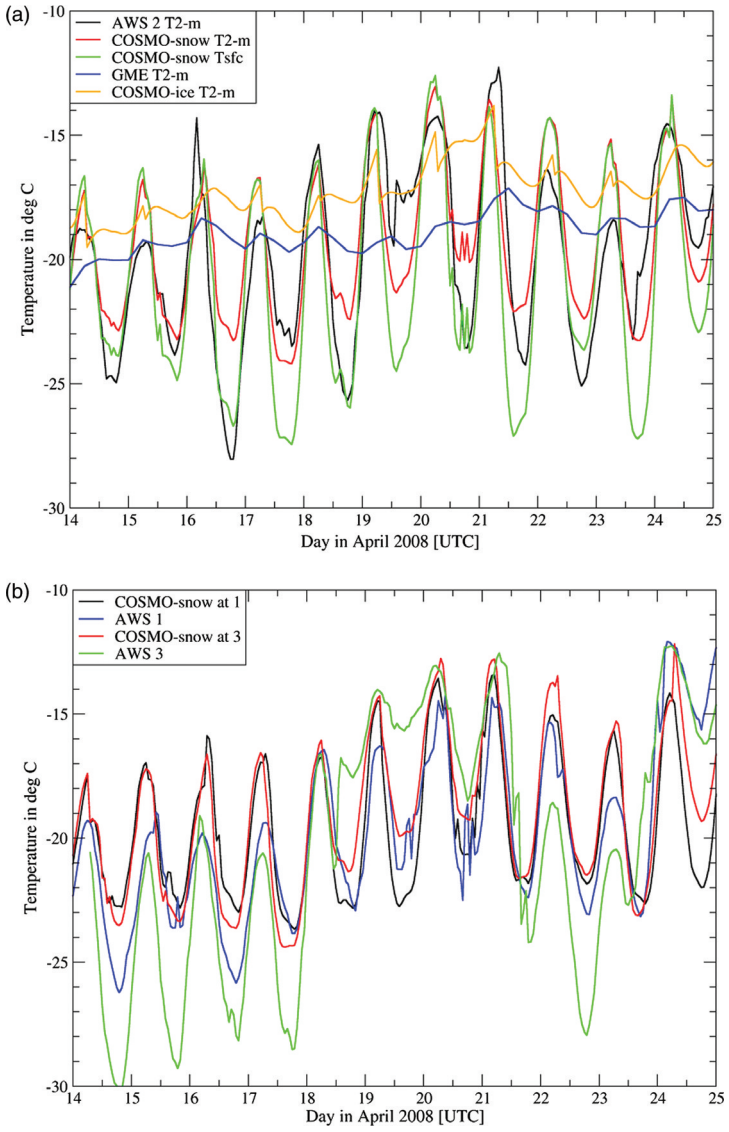

Fig. 3 Comparison between simulated and observed 2-m air temperature at (a) automatic weather station 2 for the Global Model Extended system (GME) and different COSMO-05km sea-ice module versions and (b) at automatic weather station (AWS) 1 and 3 for GME and COSMO-snow for the period 14–25 April 2008. The simulated surface temperature is added in (a).

Table 2 Comparison between observed (automatic weather stations [AWS]) and simulated (COSMO-snow and COSMO-ice) 2-m air temperature: mean values, bias, root mean square error (RMSE), correlation coefficient (*r*) and mean of diurnal cycle. Statistics are calculated from hourly data during 14–25 April 2008.

2-m temperature in °C	Mean	Bias	RMSE	*r*	Mean of diurnal cycle
AWS 1	−19.8	—	—	—	7.0
COSMO-snow	−19.5	+0.3	2.3	0.71	6.3
COSMO-ice	−17.3	+2.5	3.7	0.63	1.8
AWS 2	−19.8	—	—	—	7.9
COSMO-snow	−19.4	+0.4	2.1	0.81	7.2
COSMO-ice	−17.2	+2.6	4.1	0.41	1.8
AWS 3	−20.2	—	—	—	8.6
COSMO-snow	−19.2	+1.0	3.6	0.76	7.3
COSMO-ice	−16.9	+3.3	5.3	0.72	1.9

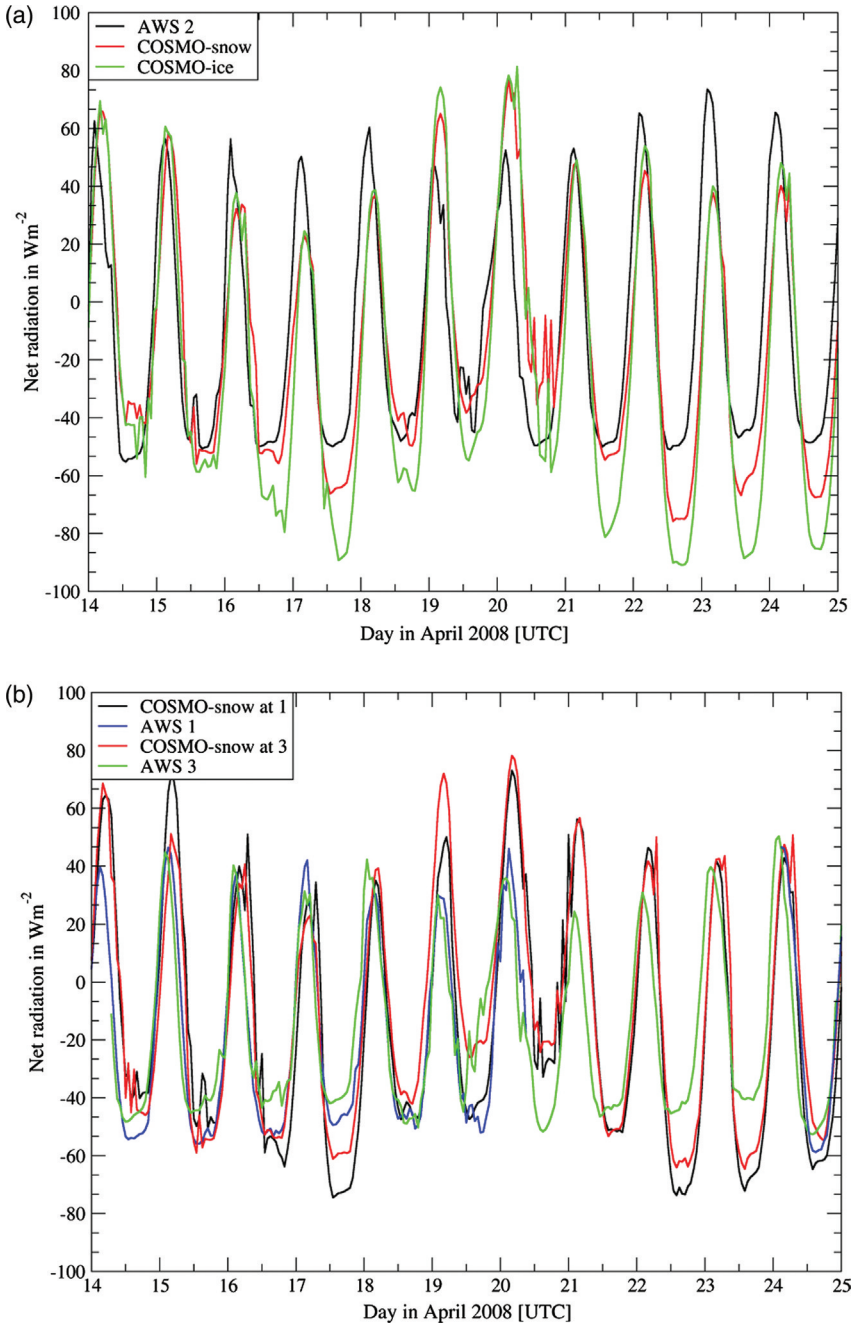

Fig. 4 Comparison between simulated and observed surface net radiation at (a) automatic weather station (AWS) 2 for the Global Model Extended system (GME) and different COSMO-05km sea-ice module versions and (b) at AWS 1 and 3 for GME and COSMO-snow for the period 14–25 April 2008. For the period 20 April 12 UTC to 24 April 00 UTC no data are available from AWS 1.

snow layer, as done in the COSMO-snow runs (Fig. 3). In comparison to the COSMO-ice run, the absolute error reduces from +2.6 K to +0.4 K and the RMS errors from 4.1 K to 2.1 K (Table 2). The correlation coefficient improves from 0.41 to 0.81. The mean diurnal circle increases from 1.8 K to 7.2 K, which is very close to the observed one of 7.9 K (based on hourly data). The agreement of 2-m air temperature between observations and the COSMO-snow run is remarkable considering that this quantity is very sensitive to wind speed and cloud cover. The simulated surface temperature is shown in Fig. 3a. During the day, surface and 2-m air temperature are within 1 K, but during nights the simulated surface temperature can be up to 5 K lower.

Citation: *Polar Research* 2011, *30*, 6334, DOI: 10.3402/polar.v30i0.6334

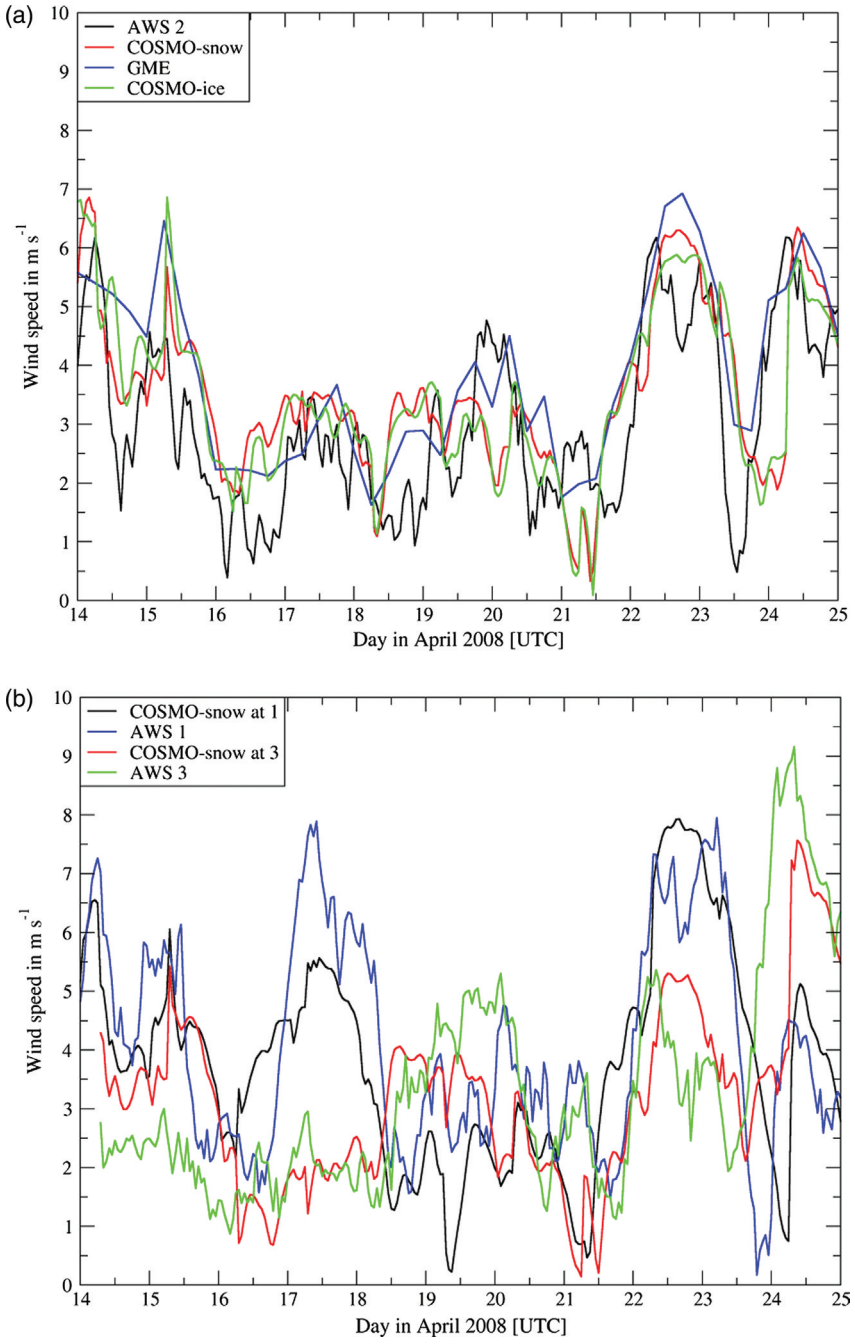

Fig. 5 Comparison between simulated and observed 10-m wind speed at (a) automatic weather station (AWS) 2 for the Global Model Extended system (GME) and different COSMO-05km sea-ice module versions and (b) at AWS 1 and 3 for GME and COSMO-snow for the period 14–25 April 2008.

When AWS 1 and AWS 3 are included in the comparison (Fig. 3b), it is striking that there are clear differences between the observations themselves, which are only 120 km apart. For example, the minimum temperature of the most northern AWS 3 is 5 K lower than AWS 1 and 2 during the first two nights. The simulated temperature shows lower spatial differences.

Surface net radiation. The simulated surface net radiation is shown for comparison with the observed balance for AWS 2 in Fig. 4a. The absolute errors for the whole period are small (-4 Wm^{-2} for COSMO-snow at AWS 2; Table 3), the RMS errors amount to 24 Wm^{-2} (COSMO-snow) and 31 Wm^{-2} (COSMO-ice) and the correlation coefficients are 0.81 and 0.80, respectively.

Table 3 Comparison between observed (automatic weather stations [AWS]) and simulated (COSMO-snow and COSMO-ice) surface net radiation: mean values, bias, root mean square error (RMSE), correlation coefficient (*r*) and mean of diurnal cycle. Statistics are calculated from hourly data during 14–25 April 2008.

Net radiation in W m^{-2}	Mean	Bias	RMSE	*r*	Mean of diurnal cycle
AWS 1	−44	—	—	—	90
COSMO-snow	−14	+30	22	0.50	105
COSMO-ice	−21	+23	27	0.52	129
AWS 2	−10	—	—	—	108
COSMO-snow	−14	−4	24	0.81	104
COSMO-ice	−22	−12	31	0.80	128
AWS 3	−17	—	—	—	83
COSMO-snow	−11	+6	26	0.76	100
COSMO-ice	−21	−4	32	0.77	125

The observed mean diurnal circle of 108 Wm^{-2} is well simulated in COSMO-snow (104 Wm^{-2}), but is overestimated in COSMO-ice (128 Wm^{-2}). The good agreement of the diurnal cycle demonstrates that our approach is suitable to keep the temperature between ice and snow constant for a 30-hour-long run and only to take into account the heat capacity of the snow layer. Remaining differences can be explained by wrong cloudiness (e.g., 17 and 18 April) and by the impact of the GME surface temperature that is applied for the constant ice–snow temperature. In cases where the GME daily mean air temperature is close to observations (e.g., 14 April or 21 April; Fig. 3a) and therefore the GME daily mean surface temperature is close to reality, net radiation fluxes agree within the range of measurement uncertainty (Fig. 4a). In cases where the GME daily mean temperature is too high (e.g., 23 April; Fig. 3a) the simulated net radiation is too low (Fig. 4a) and vice versa (e.g., 19 April). These findings are confirmed by the comparison of the other stations (Fig. 4b).

10-m wind speed. As discussed earlier, GME wind speed matches the observations quite well and no major modifications occur in the COSMO simulations (Fig. 5). Nevertheless, a few differences regarding air temperature can be explained by errors in wind speed. On 16 April the observed wind speed varies between 0.5 ms^{-1} and 2 ms^{-1} (Fig. 5a), whereas the simulated wind speed is between 2 ms^{-1} and 3.5 ms^{-1} (Fig. 5a). Higher wind speeds increase the turbulent mixing, which reduces the local cooling during the night and the heating during the day. This results in an underestimation of maximum temperature (−16.5°C instead of −14°C; Fig. 3a) and an overestimation of minimum temperature (−23.5°C instead of −28°C; Fig. 3a).

Impact of sea-ice parameterization on spatial variability

The agreement between observations and simulations along the western New Siberian polynya does not guarantee that the simulations are accurate for the whole Laptev Sea. To verify surface temperature for the whole Laptev Sea we can access five MODIS scenes in the second half of April 2008. The derived surface temperature fields, at a spatial resolution of 1 km, are interpolated onto the COSMO-05km grid and compared with COSMO simulations. We assume a total accuracy of the MODIS-based surface temperature of 2–3 K. Errors are caused by uncertainties of the algorithm (see Hall et al. 2004 for details) and by a time shift of up to 30 min between the MODIS scenes and the hourly simulation data: temporal changes of ice-surface temperature can be up to 4 K/hour (Fig. 3b). Surface temperature distributions are shown for 11 UTC (19 LT) on 29 April 2008 in Fig. 6. According to MODIS, the surface temperature reveals three features (Fig. 6a): first, there is a general gradient with higher temperatures in the south (−13°C) and lower temperatures in the north (−17°C). Second, the polynya itself is characterized by a surface temperature between −2°C and −7°C, so just a small part seems to be ice-free. Third, there is an area west of the polynya where the surface temperature is higher (−12°C) due to the polynya and the easterly winds. Features one and three are well simulated by COSMO-snow (Fig. 6b, c), apart from the northern edge, where the temperature is overestimated by 2–4 K due to clouds in the simulation (small map in Fig. 6b). The polynya is ice-free in the simulation and a water temperature of −1.8°C is prescribed. In the COSMO-ice simulation, surface temperature decreases too slowly in the evening (19 LT) and is therefore overestimated by 2–6 K (Fig. 6d, e).

Citation: *Polar Research* 2011, *30*, 6334, DOI: 10.3402/polar.v30i0.6334

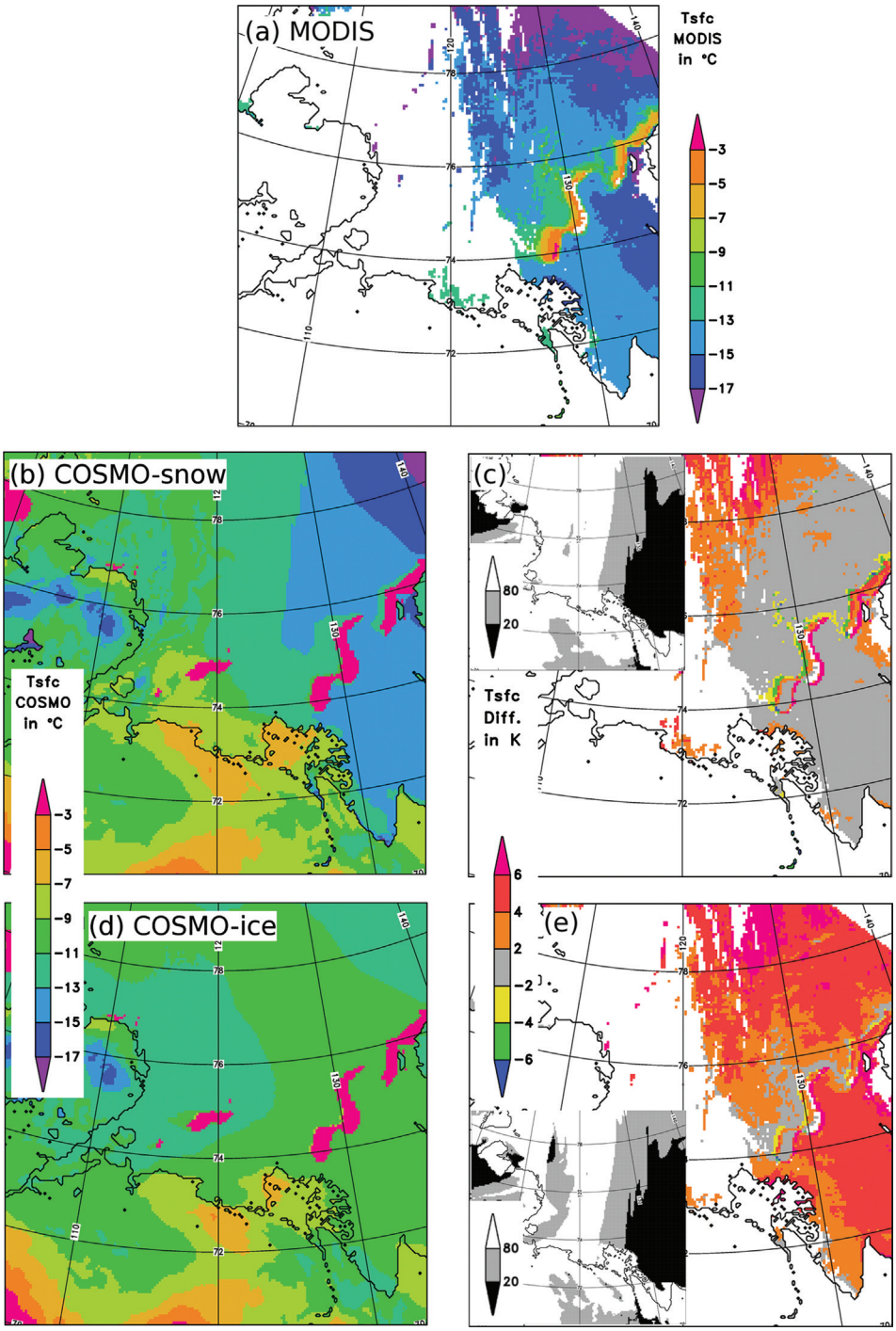

Fig. 6 Surface temperature (T_{sfc}) at 11 UTC (19 LT) on 29 April 2008: (a) Moderate Resolution Imaging Spectroradiometer (MODIS) satellite data, (b) COSMO-snow and (d) COSMO-ice. Differences are shown in (c) and (e) with respect to MODIS. Simulated total cloud cover (clct) is shown in the small maps in (c) and (e): clct >80% in white and clct <20% in black.

The differences between COSMO-snow and MODIS are shown for the other four MODIS scenes in Fig. 7. Surface temperature is overestimated by more than 2 K in the simulation in some regions. A comparison of the differences of surface temperature with total cloud cover (small maps in Fig. 7) reveals that larger differences occur in regions that are clouded in the model. In reality, there are no clouds: surface temperature is only

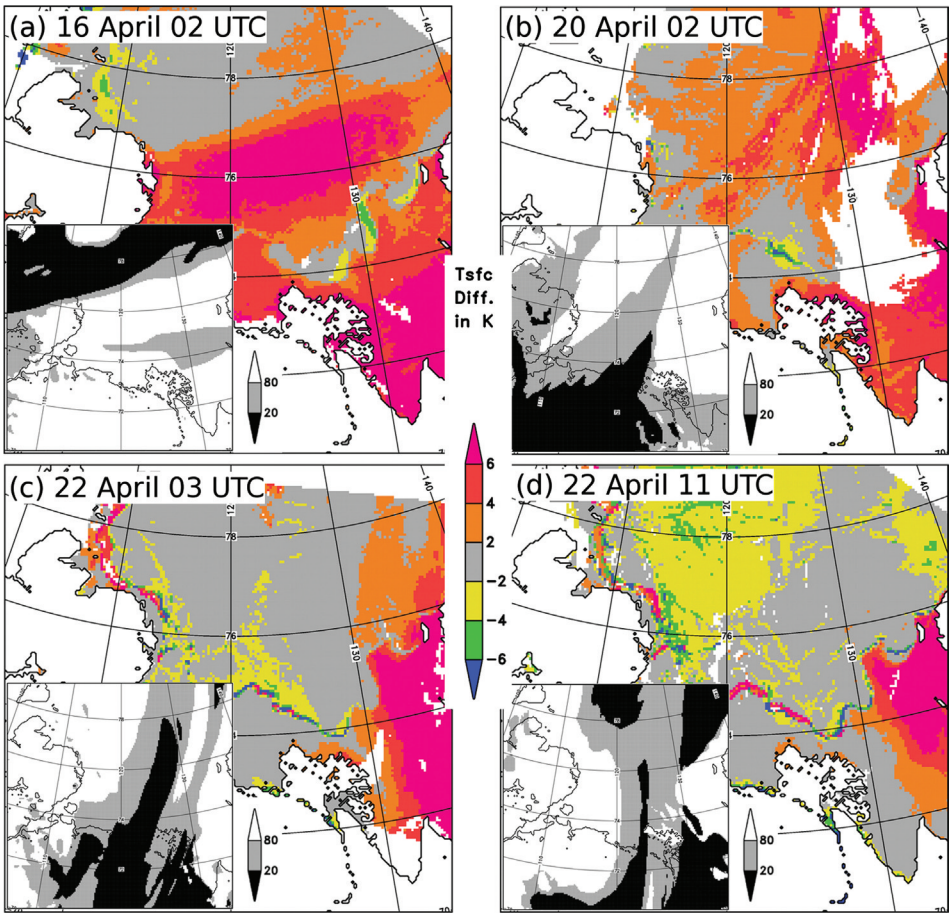

Fig. 7 Differences between simulated (COSMO-snow) and Moderate Resolution Imaging Spectroradiometer (MODIS) surface temperature (T_{sfc}): (a) at 02 UTC (10 LT) on 16 April, (b) at 02 UTC (10 LT) on 20 April, (c) at 03 UTC (11 LT) on 22 April and (d) at 11 UTC (19 LT) on 22 April. Simulated total cloud cover (clct) is shown is shown in the small maps: clct >80% in white and clct <20% in black.

available from MODIS for cloud-free regions. Therefore, the temperature differences are caused by errors in simulated cloudiness. If no modelled clouds are present, there is a good agreement between observations and simulations supporting the performance of the implemented sea-ice module. The good agreement is confirmed by statistical analysis (Table 4). Taking into account all grid points (approximately 90 000 cases at five dates), the observed temperature mean of −19.0°C is overestimated in the COSMO-snow simulation by 1.4 K with a RMS value of 3.3 K and a correlation coefficient of 0.58. Restricting the comparison to cloud-

Table 4 Comparison between observed (Moderate Resolution Imaging Spectroradiometer [MODIS] satellite data) and simulated (COSMO-snow and COSMO-ice) surface temperature; standard deviation (SD) describes the internal variability of each data set. Bias, root mean square error (RMSE) and correlation coefficient (*r*) are calculated for the comparison with MODIS data. As indicated in the second column, statistics are based on all 89 563 grid points of five dates (see Figs. 6, 7) and on all cases with simulated total cloud cover (clct) <20% (20 244 cases in COSMO-snow and 20 612 cases in COSMO-ice).

Tsfc in °C		Mean	SD	BIAS	RMSE	*r*
MODIS	Total	−19.0	4.4	—	—	—
	clct <20%	−19.0	4.9			
COSMO-snow	Total	−17.6	3.8	+1.4	3.3	0.58
	clct <20%	−19.2	4.5	−0.2	2.7	0.84
COSMO-ice	Total	−17.0	3.5	+2.0	4.2	0.48
	clct <20%	−16.7	4.4	+2.3	4.5	0.63

Citation: *Polar Research* 2011, *30*, 6334, DOI: 10.3402/polar.v30i0.6334

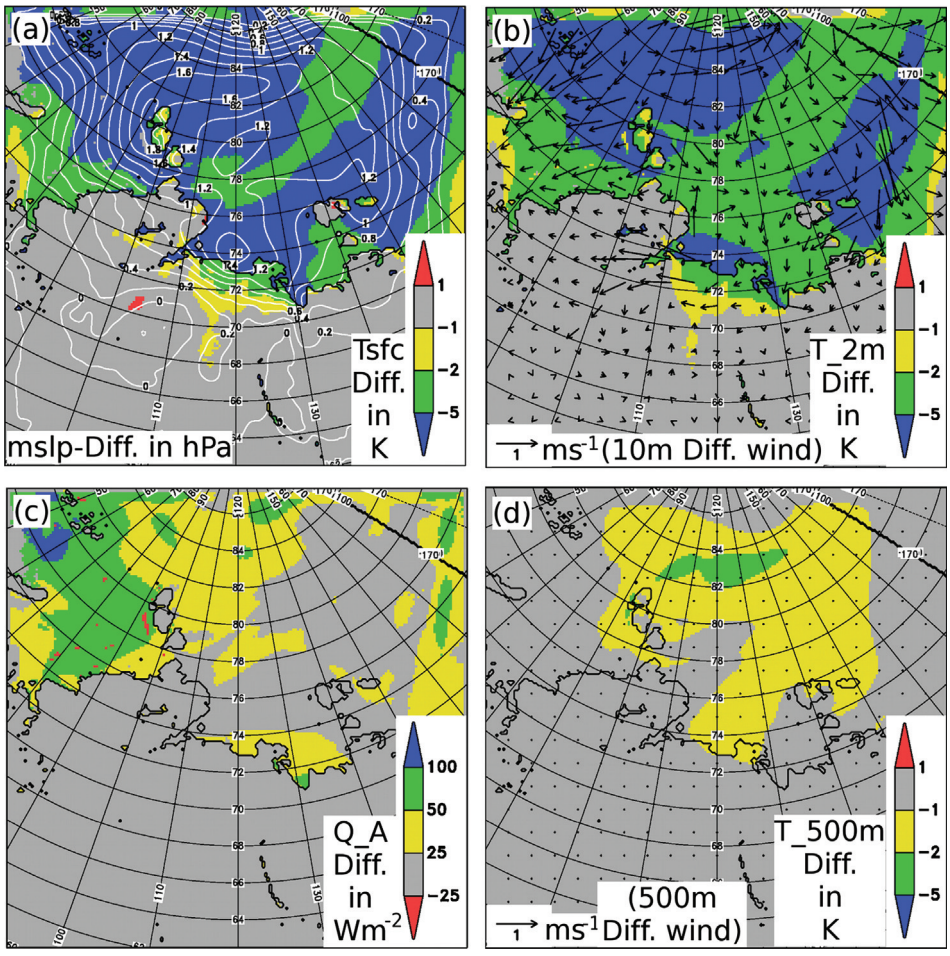

Fig. 8 Differences on the fifth simulation day (18 April 2008, 24-hour mean) between COSMO-snow-5 days and COSMO-ice-5 days (15 km resolution): (a) surface temperature (T_{sfc}) (coloured) and mean sea-level pressure (mslp) (contours), (b) 2-m air temperature (T_2 m) (coloured) and 10-m wind vector, (c) total atmospheric heat flux (Q_A) and (d) 500-m air temperature (T_500 m) (coloured) and 500-m wind vector.

free cases (approximately 20 000 cases), the mean values differ by just 0.2 K, the RMS error is reduced to 2.7 K (within the range of uncertainty of MODIS temperature) and the correlation coefficient increases to 0.84. COSMO-ice results are worse (RMS error value of 4.5 K, correlation coefficient of 0.63), but nevertheless much better than a constant surface temperature.

How important is an accurate simulation of surface temperature? To answer this question we compare two five-day simulations on the COSMO-15 km grid: COSMO-ice-5 days and COSMO-snow-5 days (see earlier description). The differences on the fifth day (18 April 2008) are shown in Fig. 8. Sea-ice temperature is 5 K colder in COSMO-snow-5 days in comparison to COSMO-ice-5 days (Fig. 8a). This leads to a decrease of 2-m temperature of nearly the same magnitude (Fig. 8b) and to an increase of mean sea-level pressure of up to 1.5 hPa (Fig. 8a). Local changes of wind vector occur with a maximal anomalous wind speed of 2 ms^{-1} (Fig. 8b). The impact on the total atmospheric heat flux differs regionally (Fig. 8c). In the northern Laptev Sea the differences between both runs are small; however, differences of up to more than 100 Wm^{-2} (as a daily mean) occur over the northern Barents Sea. In contrast to the strong impact on the near surface conditions over ice and on the surface heat balance, changes at higher levels are less pronounced (Fig. 8d). The temperature differences at a height of 500 m hardly exceed 2 K and there are no significant changes for the wind vector and for all parameters at levels above 500 m. Differences are regarded as significant if they are larger than the "signal of noise"; that is, the difference caused by internal variability. Based on comparisons between identically configured runs starting on different dates, we identify differences of more than 1 K and of more than 25 Wm^{-2} as significant.

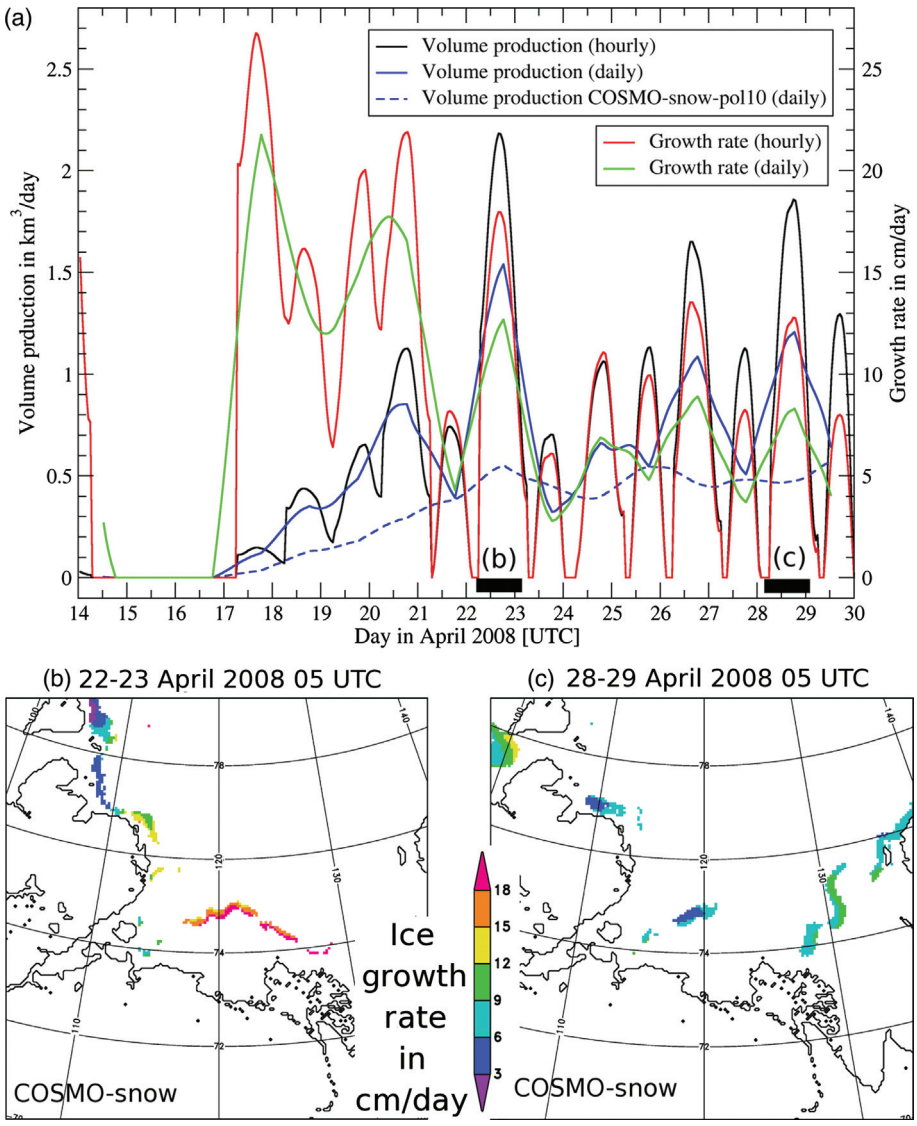

Fig. 9 Sea-ice production in Laptev Sea polynyas: (a) time series of total volume production and mean ice growth rate based on COMSO-snow (continuous lines) and COSMO-snow-pol10 (dashed line) simulations for the period 14–30 April 2008. Spatial distributions of daily mean ice growth rate for polynya events on (b) 22/23 April and (c) 28/29 April.

In summary, the comparison shows that the atmospheric circulation mainly depends on the boundary data (GME analyses in both cases), but an accurate surface temperature is essential for the near surface conditions and for calculating the surface energy balance over the ocean.

Application: sea-ice production in the Laptev Sea polynyas

Following a commonly used approach (e.g., Dethleff et al. 1998; Martin et al. 2007; Tamura et al. 2008), sea-ice production in the polynyas is estimated from a heat flux conversion by assuming the total atmospheric heat flux (sum of surface net radiation balance and turbulent surface fluxes of sensible and latent heat) is balanced by ice growth. Thus, the ice growth rate is given by:

$$\frac{\partial h_i}{\partial t} = -\frac{Q_A}{\rho_i \cdot L_f}. \qquad (6)$$

The ice-volume production is then calculated as the integral of the growth rate over the polynya area. During winter/springtime, the upper ocean layer is close to the freezing point and, thus, the oceanic heat flux is small and can be neglected. We apply the atmospheric heat

Citation: *Polar Research* 2011, *30*, 6334, DOI: 10.3402/polar.v30i0.6334

fluxes from the COSMO-snow simulation to calculate sea-ice production for the period 14–30 April 2008. As described above, the polynya areas are prescribed daily and kept constant for 24 hours. This implicitly assumes that the produced ice does not accumulate in the polynya. In reality, grease ice or thin ice can form depending on wind speed and air temperature, which might reduce the absolute value of the total atmospheric heat flux. Thus, our estimation is an upper limit and represents potential sea-ice production.

The ice-volume production of the total Laptev Sea varies between 0 and 1.5 km^3/day during 14–30 April (Fig. 9a). The maximum production occurs on 22 April. The polynya areas vary depending on wind direction. On 22/23 April, sea ice is produced in the Anabar–Lena polynya and the eastern Severnaya Zemlya polynya (Fig. 9b). This is due to southerly winds. During the end of April, the western New Siberian polynya is the largest (Fig. 9c). This is caused by easterly winds. The strongest growth rate occurs on 17 April, with a daily mean of 21 cm/day, but due to a small polynya area the ice volume produced is small. There is a pronounced daily cycle with no ice production during noon from 21 April onwards.

The average total production rate of 0.53 km^3/day in the second half of April 2008 is smaller than winter averages in the literature. Dethleff et al. (1998) estimated a winter ice-volume production of 258 km^3, which is equivalent to an average production rate of 1.43 km^3/day. Using measurements of changes in salinity, Dmitrenko et al. (2009) derived a mean annual ice production of more than 1000 km^3 for the whole Laptev Sea. On the other hand, our value of 0.53 km^3/day is three times larger than the sea-ice production rate of 0.17 km^3/day for the same period calculated by the method of Willmes et al. (2011). Using AMSR-E and National Centers for Environmental Prediction reanalyses data, Willmes et al. detected that most parts of the Laptev Sea polynyas are not ice-free. They derived a mean ice thickness of 10 cm over the polynyas. Performing simulations with 10-cm ice instead of ice-free polynyas (COSMO-snow-pol10), we came up with a mean production rate that decreased from 0.53 km^3/day to 0.30 km^3/day (Fig. 9a).

Summary and conclusions

We have implemented a thermodynamic sea-ice module in the NWP model COSMO. The module provides two prognostic variables: sea-ice surface temperature and sea-ice thickness. The impact of a snow layer is accounted for by using different thermal characteristics. Simulations have been performed for the Laptev Sea using a model chain: global GME analyses (40-km mesh size); COSMO runs with a mesh size of 15 km for a 3000 km × 3000 km area; and COSMO runs with a mesh size of 5 km for a 1000 km × 1000 km area covering the Laptev Sea.

Four AWS were deployed along the edge of the western New Siberian polynya from 11 to 29 April 2008 during the Transdrift XIII-2 expedition. These in situ data enable us to verify modelled 2-m air temperature, 2-m air humidity, mean sea-level pressure, 10-m wind vector and surface net radiation. The GME analyses depict the synoptic weather situation well, but the diurnal cycle of 2-m air temperature is not captured (0.7 K instead of 6.0 K for AWS 2 based on six-hourly data). This seems to be caused by the missing snow treatment in the sea-ice module of GME. When the same sea-ice module in higher resolution COSMO simulations (COSMO-ice) is applied, sub-daily variability of 2-m air temperature is still strongly underestimated. However, by accounting for a snow layer (COSMO-snow), the observed variability of air temperature and surface net radiation is realistically simulated. The mean modelled diurnal cycle of 7.2 K for AWS 2 is close to the observed one of 7.9 K based on hourly data, and the RMS error amounts to 2.1 K. The realistic simulation of 2-m air temperature implies a realistic evaluation of sea-ice surface temperature.

Surface temperature is available from MODIS satellite data under clear-sky conditions at a horizontal resolution of 1 km. Five data sets from the second half of April 2008 can be used to verify the spatial variability of simulated sea-ice surface temperature. Mean simulation value and standard deviation (-19.2 ± 4.5 K) are in agreement with remote sensing data (-19.0 ± 4.9 K). The RMS error of 2.7 K is in the range of the accuracy of the MODIS data. The correlation coefficient is 0.84 for 20 000 clear-sky model grid boxes. This remarkable agreement demonstrates that the sea-ice module can be applied for short-range simulations. The quality of the model results naturally depends on the quality of the boundary data—in our case mainly of the prescribed sea-ice cover. Additional simulations for various winter months (not shown) reveal that sea-ice surface temperatures are only simulated realistically provided that AMSR data capture the polynyas properly and that the lateral boundary data from the global model are adequate.

Comparing five-day simulations with the implemented sea-ice module Option A (COSMO-ice-5 days) and Option B (COSMO-snow-5 days) shows that an accurate sea-ice surface temperature is essential for simulating

realistic near-surface conditions and the surface energy balance, which is important for many scientific questions.

The key question for the Laptev Sea is to quantify the ice production in the polynyas (Rigor & Colony 1997; Dethleff et al. 1998; Alexandrov et al. 2000; Morales Maqueda et al. 2004; Bareiss & Görgen 2005). Assuming that the total atmospheric heat flux over polynyas is balanced by ice growth, potential sea-ice production can be derived from Eqn. 6 by applying the atmospheric heat fluxes from COSMO-snow. For the period 14–20 April 2008, the maximum daily mean growth rate is 22 cm/day and the average volume production rate amounts to 0.53 km^3/day for all Laptev Sea polynyas together. Assuming the polynyas are not ice-free but covered by a 10-cm thin ice layer (COSMO-snow-pol10), our production rate reduces to 0.30 km^3/day. Discrepancies in ice production between our results and the estimation of Dethleff et al. (1998), Dmitrenko et al. (2009) and Willmes et al. (2011) reveal the uncertainties of different methods. In previous studies, one major source of error is the atmospheric heat flux being calculated from station (Dethleff et al. 1998) or reanalysis data (Willmes et al. 2011) that do not involve polynya signatures. Our model studies show that 2-m air temperature and 10-m wind speed are frequently more than 10 K higher and 3 m s^{-1} stronger above the polynya than above the land-fast ice within a distance of just 10 km. Accounting for the influence of the polynya on the atmospheric conditions, more accurate heat fluxes are simulated by our COSMO-snow runs. We prescribed the polynya areas daily and kept them constant for 24 hours such that sub-daily variability is not accounted for. However, because the mean duration of Laptev Sea polynyas is 13–22 days, the induced error is minor (Bareiss & Görgen 2005).

Our COSMO-snow simulations provide a high-resolution and high-quality atmospheric data set for the Laptev Sea region in April 2008. By extending the simulations to longer periods, COSMO with the implemented sea-ice module will be used to quantify sea-ice production and the role of the Laptev Sea in the Arctic sea-ice budget more accurately. COSMO-ice is applied for idealized case studies by Ebner et al. (2011 [this volume]) and further applications are underway. The sea-ice module is now integrated into the latest version of the COSMO model (version 4.12) and is available for all COSMO users.

Acknowledgements

We are grateful to colleagues who participated in the field experiment 2008, particularly Alfred Helbig and Thomas Ernsdorf. The COSMO model and GME analyses were made available by the German Weather Service. The support by Dimitrii Mironov and Jan-Peter Schulz is acknowledged. AMSR-E data were provided by the University of Hamburg and MODIS thermal infrared satellite data by NASA. This study was funded by the German Ministry for Education and Research project Laptev Sea System (grant no. 0360639E).

References

Alexandrov V.Y., Martin T., Kolatschek J., Eicken H., Kreyscher M. & Makshtas A.P. 2000. Sea ice circulation in the Laptev Sea and ice export to the Arctic Ocean: results from satellite remote sensing and numerical modeling. *Journal of Geophysical Research—Oceans 105*, 143–159.

Barber D.G. & Massom R.A. 2007. The role of sea ice in Arctic and Antarctic polynyas. In W.O. Smith Jr. & D.G. Barber (eds.): *Polynyas: windows to the world*. Pp. 1–43. Amsterdam: Elsevier.

Bareiss J. & Görgen K. 2005. Spatial and temporal variability of sea ice in the Laptev Sea: analyses and review of satellite passive-microwave data and model results, 1979 to 2002. *Global and Planetary Change 48*, 28–54.

Bentamy A., Croize-Fillon D., Queffeulou P., Liu C. & Roquet H. 2009. Evaluation of high-resolution surface wind products at global and regional scales. *Journal of Operational Oceanography 2(2)*, 15–27.

Bromwich D.H. & Wang S.-H. 2005. Evaluation of the NCEP-NCAR and ECMWF 15- and 40-yr reanalyses using raw-insonde data from two independent Arctic field experiments. *Monthly Weather Review 133*, 3562–3578.

Brümmer B., Schröder D., Launiainen J., Vihma T., Smedman A.-S. & Magnusson M. 2002. Temporal and spatial variability of surface fluxes over the ice edge zone in the northern Baltic Sea. *Journal of Geophysical Research—Oceans 107*, article no. 3096, doi: 10.1029/2001JC000884.

Charnock H. 1955. Wind stress over a water surface. *The Quarterly Journal of the Royal Meteorological Society 81*, 639–640.

Dethleff D., Loewe P. & Kleine E. 1998. The Laptev Sea flaw lead—detailed investigations on ice formation and export during 1991/1992 winter season. *Cold Regions Science and Technology 27*, 225–243.

Dmitrenko I.A., Kirillov S.A., Tremblay B., Bauch D. & Willmes S. 2009. Sea-ice production over the Laptev Sea shelf inferred from historical summer to winter hydrographic observations of 1960s–1990s. *Geophysical Research Letters 36*, L13605, doi: 10.1029/2009GL038775.

Ebner L., Schröder D. & Heinemann G. 2011. Impact of Laptev Sea polynyas on the atmospheric boundary layer and ice production using idealized mesoscale simulations. *Polar Research 30*, 6334, doi: 10.3402/polar.v30i0.6334 (this volume).

Elementi M., Marsigh C. & Paccagnella T. 2005. High resolution forecast of heavy precipitation with Lokal Modell:

analysis of two case studies in the alpine area. *Natural Hazards and Earth System Sciences 5*, 593–602.

Grützun V., Knoth O. & Simmel M. 2008. Simulation of the influence of aerosol particle characteristics on clouds and precipitation with LM-SPECS: model description and first results. *Atmospheric Research 90*, 233–242.

Hall D.K., Key J.R., Casey K.A., Riggs G.A. & Calavieri D.J. 2004. Sea ice surface temperature product from MODIS. *IEEE Transactions on Geoscience and Remote Sensing 42*, 1076–1087.

Hebbinghaus H. & Heinemann G. 2006. LM simulations of the Greenland boundary layer, comparison with local measurements and SNOWPACK simulations of drifting snow. *Cold Regions Science and Technology 46*, 36–51.

Heinemann G., Helbig A. & Ernsdorf T. 2009. Meteorological measurements at the ice edge of the West New Siberian Polynya. In: *Russisch–Deutsche Zusammenarbeit: System Laptev-See, Zwischenbericht 2008, Fahrtbericht der Expedition Transdrift XIII. (Russian–German Cooperation: System Laptev Sea, report 2008, the cruise report of the Transdrift XIII expedition*.) Pp. 8–19. Kiel, Germany: Secretariat of the Laptev Sea System, IFM-GEOMAR.

Heise E., Ritter B. & Schrodin R. 2006. *Operational implementation of the multilayer soil model. COSMO Technical Reports No. 9.* Offenbach om Main, Germany: Consortium for Small-scale Modelling.

Key J., Collins J., Fowler C. & Stone R. 1997. High-latitude surface temperature estimates from thermal satellite data. *Remote Sensing of Environment 61*, 302–309.

Klein T., Heinemann G. & Gross P. 2001. Simulation of the katabatic flow near the Greenland ice margin using a high-resolution nonhydrostatic model. *Meteorologische Zeitschrift 10*, 331–339.

Klemp J.B. & Wilhelmson R. 1978. The simulation of three-dimensional convective storm dynamics. *Journal of the Atmospheric Sciences 35*, 1070–1096.

Kolstad E.W. 2008. A QuikSCAT climatology of ocean surface winds in the Nordic seas: identification of features and comparison with the NCEP/NCAR reanalysis. Journal of Geophysical Research—Atmospheres *113*, D11106, doi: 10.1029/2007JD008918.

Louis J.-F. 1979. A parametric model of vertical eddy fluxes in the atmosphere. *Boundary-Layer Meteorology 17*, 187–202.

Majewski D., Liermann D., Prohl P., Ritter B., Buchhold M., Hanisch T., Paul G., Wergen W. & Baumgardner J. 2002. The Operational Global Icosahedral–Hexagonal Gridpoint Model GME: description and high-resolution tests. *Monthly Weather Review 130*, 319–338.

Male D.H. 1980. The seasonal snowcover. In S.C. Colbeck (ed.): *Dynamics of snow and ice masses*. Pp. 305–395. San Francisco, CA: Academic Press.

Martin S., Drucker R.S. & Kwok R. 2007. The areas and ice production of the western and central Ross Sea polynyas, 1992–2002, and their relation to the B-15 and C-19 iceberg events of 2000 and 2002. *Journal of Marine Systems 68*, 201–214.

Massom R.A., Harris P.T., Michael K. & Potter M.J. 1998. The distribution and formative processes of latent heat polynyas in East Antarctica. *Annals of Glaciology 27*, 420–426.

Mironov D. & Ritter B. 2004. *A new sea ice model for GME. Technical note*. Offenbach am Main, Germany: Deutscher Wetterdienst.

Morales Maqueda M.A., Willmott A.J. & Biggs N.R.T. 2004. Polynya dynamics: a review of observations and modeling. *Reviews of Geophysics 42*, RG1004, doi: 10.1029/2002RG000116.

Muhlbauer A. & Lohmann U. 2008. Sensitivity studies of the role of aerosols in warm-phase orographic precipitation in different dynamical flow regimes. *Journal of the Atmospheric Sciences 65*, 2522–2542.

Parmiggiani F. 2006. Fluctuations of Terra Nova Bay polynya as observed by active (ASAR) and passive (AMSR-E) microwave radiometers. *International Journal of Remote Sensing 27*, 2459–2469.

Rigor I.G. & Colony R. 1997. Sea ice production and transport of pollutants in the Laptev Sea, 1979–2003. *Science of the Total Environment 202*, 90–110.

Rinke A. & Dethloff K. 2001. On the sensitivity of a regional Arctic climate model to initial and boundary conditions. *Journal of Climate Research 14*, 101–113.

Ritter B. & Geleyn J.-F. 1992. A comprehensive radiation scheme for numerical weather prediction models with potential applications in climate simulations. *Monthly Weather Review 120*, 303–325.

Schättler U., Doms G. & Schraff C. 2008. *A description of the nonhydrostatic regional COSMO-model. Part vii: user's guide*. Offenbach am Main, Germany: Deutscher Wetterdienst.

Spreen G., Kaleschke L. & Heygster G. 2008. Sea ice remote sensing using AMSR-E 89 GHz channels. *Journal of Geophysical Research—Oceans 113*, C02S03, doi: 10.1029/2005JC003384.

Stephan K., Klink S. & Schraff C. 2008. Assimilation of radar-derived rain rates into the convective-scale model COSMO-DE at DWD. *Quarterly Journal of the Royal Meteorological Society 134*, 1315–1326.

Steppeler J., Doms G., Schättler U., Bitzer H.W., Gassmann A., Damrath U. & Gregoric G. 2003. Meso-gamma scale forecasts using the nonhydrostatic model LM. *Meteorology and Atmospheric Physics 82*, 75–96.

Tamura T., Ohshima K.I. & Nihashi S. 2008. Mapping of sea ice production for Antarctic coastal polynyas. *Geophysical Research Letters 35*, L07606, doi: 10.1029/2007GL032903.

Tiedtke M. 1989. A comprehensive mass flux scheme for cumulus parameterization in largescale models. *Monthly Weather Review 117*, 1779–1800.

Timmermann R., Bechmann A. & Helmer H.H. 2002. Simulations of ice–ocean dynamics in the Weddell Sea 1. Model configuration and validation. *Journal of Geophysical*

Research—Oceans 107, article no. 3024, doi: 10.1029/2000Jc000741.

Wacker U., Potty K.V.J., Lüpkes C., Hartmann J. & Raschendorfer M. 2005. A case study on a polar cold air outbreak over Fram Strait using a mesoscale weather prediction model. *Boundary-Layer Meteorology 117*, 301–336.

Wicker L. & Skamarock W. 2002. Time splitting methods for elastic models using forward time schemes. *Monthly Weather Review 130*, 2088–2097.

Willmes S., Adams S., Schröder D. & Heinemann G. 2011. Spatiotemporal variability of sea-ice coverage, polynya dynamics and ice production in the Laptev Sea between the winters of 1979/80 and 2007/08. *Polar Research 30*, article no. 5971, doi: 10.3402/polar.v30i0.5971 (this volume).

Zakharov V.F. 1996. The role of flaw leads off the edge of fast ice in the hydrological and ice regime of the Laptev Sea. *Oceanology 6*, 815–821.